Structural investigation of diamond nanoplatelets grown by microwave plasma-enhanced chemical vapor deposition

Hou-Guang Chen[a] and Li Chang
Department of Materials Science and Engineering, National Chiao Tung University, Taiwan 300, Republic of China

(Received 9 February 2004; accepted 13 December 2004)

We report a unique morphology of diamond nanoplatelets synthesized by microwave plasma chemical vapor deposition on Ni coated polycrystalline diamond substrates. The diamond nanoplatelets were as thin as approximately 30 nm. Electron microscopy showed that the diamond nanoplatelets appear in a shape consisting of trapezoid and parallelogram tabular crystallites. Furthermore, the diamond nanoplatelets were single crystalline, as shown by electron diffraction. The edges of nanoplatelets were along the ⟨110⟩ direction with both the top and bottom tabular surfaces parallel to the {111} plane. Transmission electron microscopy revealed that the twinned planes are parallel to the platelet and side-face structure in ridge shape is bounded by {100} and {111} planes. Lateral growth of diamond nanoplatelet is believed to result from twin and ridge face structure. An oriented thin graphite layer was observed on some diamond nanoplatelets.

I. INTRODUCTION

Diamond is an allotrope of carbon and has many outstanding properties, such as the highest hardness, excellent thermal conductivity, biological compatibility, chemical stability, and wide band gap, etc.[1] Thus, diamond nanostructure is believed to be vitally significant for the development of nanotechnology in practical applications such as material for severe environments and biological engineering. In comparison with other biological modified materials, diamond exhibits excellent stability, sensitivity, and selectivity, all of which are necessary factors for biosensor platforms.[2] Recently, it has been predicted that diamond nanorods may have unusual mechanical properties.[3] Furthermore, diamond nanostructure is expected to play an important role for nanoelectromechanical system applications due to its high elastic modulus and strength-to-weight ratio.

Because of the high surface energy of diamond, investigation on the stability of nanoscale diamond is also attracting more attention. Theoretical prediction of stability of diamond nanostructure has been addressed.[3,4] Recently, several groups have attempted to fabricate diamond nanofibers from a diamond substrate by plasma etching[5,6] and by growth on anodic aluminum oxide templates.[7] Other nanostructured diamonds have been formed in nanoclusters by ion implantation[8] and in nanocrystalline films by chemical vapor deposition (CVD).[9] The excellent elastic, mechanical, and thermal properties of nanocrystalline diamond films have already been demonstrated.[10] Herein, we present a unique nanostructure of diamond in platelet configuration. Although the platelet morphology of diamond had been reported by Angus et al.,[11] it showed that formation of the diamond platelet with low aspect ratio was accompanied with diamond crystallites with three-dimension faceting. Also, the linear dimension of diamond platelets was on a micrometer scale. In this paper, we show that a large quantity of diamond platelets with thickness of about 30 nm can be obtained by microwave plasma chemical vapor deposition (MPCVD), and the growth mechanism of the platelets based on the results of microstructural characterization from transmission electron microsocopy (TEM) observations is discussed.

II. EXPERIMENTAL

A. Diamond nanoplatelet synthesis

A 30-μm-thick polycrystalline diamond film prepared by hot-filament chemical vapor deposition on 4-in. diameter silicon (100) wafers was used as the substrate. A 100-nm-thick nickel film was then coated on the polydiamond substrate by electron-beam evaporation. The synthesis of diamond nanoplatelets was carried out in a 2.45 GHz ASTeX (Wilmington, MA) microwave plasma CVD reactor. The substrate was placed on a graphite

[a]Address all correspondence to this author.
e-mail: houguang.mse88g@nctu.edu.tw
DOI: 10.1557/JMR.2005.0092

holder. The processing pressure was about 60 Torr, and 3% CH_4 in H_2 was used as the source gas. The input microwave power was about 800–1000 W. The substrate was immersed in the plasma to raise the temperature to above 1000 °C, as measured by an optical pyrometer. The process parameters are summarized in Table I.

B. Characterization of diamond nanoplatelets by electron microscopy

After deposition, the surface morphology was examined using a field-emission scanning electron microscope (SEM; JEOL JSM-6500F at 10 kV, Tokyo, Japan). The nanoplatelets were further characterized by TEM. A Philips Tecnai 20 (Eindhoven, The Netherlands) TEM was used for image observation and selected-area diffraction (SAD) analyses. TEM specimens were prepared by stripping the nanoplatelets off the substrate in methanol using ultrasonic vibration, followed by dragging the suspension to mount the dispersion on a TEM copper grid covered with a holey carbon film. Electron energy-loss spectroscopy (EELS) was also used to analyze the chemistry of diamond nanoplatelets. EELS was performed using a Gatan Imaging Filter (Pleasanton, CA) equipped with the TEM. In the EELS analysis, we acquired spectra in diffraction mode with a semi-collection angle approximately 3.9 mrad. High-resolution transmission electron microscopy (HRTEM) was performed on a JEOL-2010F microscope with an information limit of 0.14 nm.

III. RESULTS

A. Morphological characterization by scanning electron microscopy

The substrate obtained from hot-filament chemical vapor deposition has large grains of several tens of micrometers with facets. After 2 h MPCVD processing, a large number of nanostructures with platelet or sheetlike shape had been deposited on the original diamond substrate, and the distribution of these deposits was relatively uniform all over the substrate surface, as shown in the low-magnification SEM image of the surface in Fig. 1(a). The high-magnification picture [Fig. 1(b)] clearly reveals that these plateletlike nanostructures are standing almost perpendicularly on the substrate, and some nanoplatelets standing on the same facet of the substrate are oriented in an identical orientation. The edge dimensions of the platelets are in the range of a few hundreds of nanometers to several micrometers. In Fig. 1(c), the tabular face of these standing platelets exhibits the well-faceted morphology, suggesting that they are crystalline. Most of the nanoplatelets or nanosheets have a thickness of about 20–30 nm, as can be seen from those in the side-on orientations in Fig. 1(d) at higher magnification. SEM observations indicate that each platelet has a uniform thickness and high aspect ratio (approximately 11–90).

TABLE I. CVD process parameters.

Process parameters	Heating	Growth
Pressure (Torr)	20	60
Concentration of CH_4 in H_2(%)	0	3
Duration (min)	5	120
Total flow rate (sccm)	300	300
Microwave power (W)	800	1000
Substrate temperature (°C)	~850	>1100

B. Morphological and crystallographic characterization by TEM

Further analysis of crystallography and morphology of these nanoplatelets was carried out by TEM. Figure 2(a) is a typical bright-field (BF) image of a nanoplatelet, showing faceting at the edges with an adjacent angle of either 60° or 120°. Figure 2(b) shows that the corresponding SAD pattern can be indexed as the diffraction pattern of cubic diamond (space group $Fd3m$, $a = 0.3567$ nm) in the [111] zone-axis. The SAD pattern reveals only single-crystalline characteristics; it consists of many smaller platelets in the shape of trapezoids and parallelograms. According to SAD, all the edges of diamond nanoplatelets are along the $\langle 110 \rangle$ direction, and the top and bottom tabular surfaces are parallel to the $\{111\}$ plane. In addition to diamond diffraction spots, we also found 6-fold extra diffraction spots with weak intensity in the SAD pattern, as indicated by white arrowheads, which correspond to an interplanar spacing of 2.16 ± 0.01 Å, determined by carefully calibrated measurements. These positions are close to $1/3\{\bar{4}22\}$ forbidden reflections of diamond (0.217 nm). Such weak reflection spots can arise from the surface atomic steps[12–14] or twinned crystals.[14,15] However, such spots are also near the $10\bar{1}0$ reflections (0.213 nm) of graphite (space group $P6_3/mmc$, $a = 0.247$ nm, $c = 0.693$ nm) in the [0001] zone-axis pattern. Thus, the weak diffraction spots are probably contributed from both cases. To study the crystallographic characteristics and microstructure of the nanoplatelet, further diffraction examination in other zone-axes by tilting the TEM specimen was used. By tilting the sample about 19.5° with respect to the $[\bar{2}02]$ direction, the pattern of typical single-crystalline diamond in the [121] zone-axis can be achieved [Fig. 2(c)]. Note that the four extra spots with weak intensity in th e [121] diffraction pattern, marked by white arrowheads, are contributed from twinned diamond crystallites.[16] Then, further tilting the sample about 10.9° with respect to the $[1\bar{1}1]$ direction leads to the diffraction pattern in [231] zone-axis [Fig. 2(d)]. The characteristic twin spots of diamond can be clearly identified.[17] The hkl_T represents the Miller index of twin. Taking dark-field (DF) images from the $1\bar{1}1$ spot [Fig. 2(e)] and the $\bar{1}\bar{1}1_T$ spot

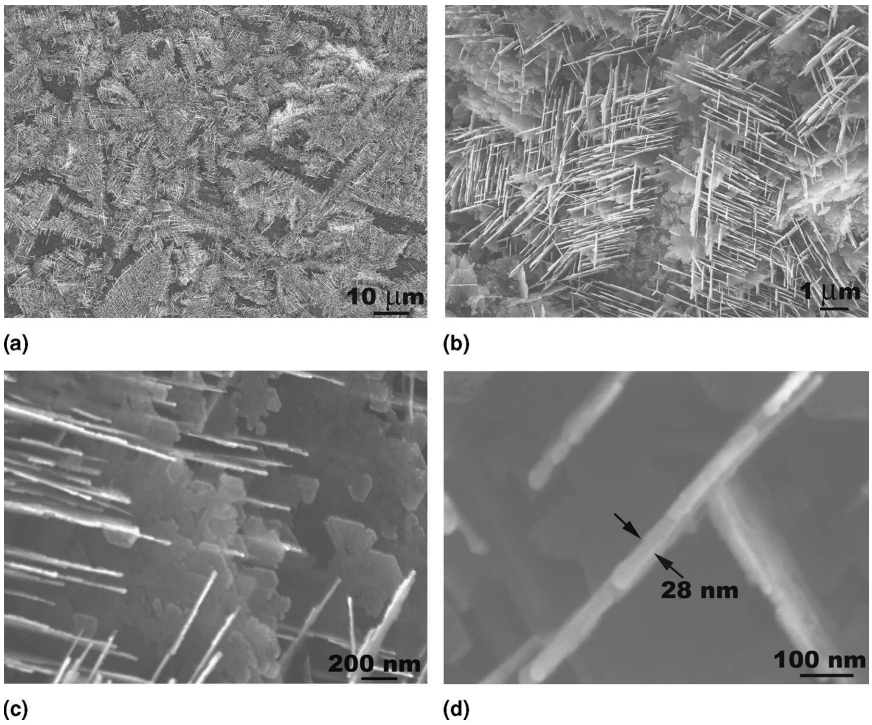

FIG. 1. (a) Low-magnification SEM micrograph showing a large number of nanostructured deposits with platelet or sheet-like configuration on the substrate. (b) Magnified SEM micrograph showing these nanostructures with platelet shape standing on the substrate. (c) Tabular face of these standing nanoplatelets with well-faceted morphology. (d) High-magnification image in side-on orientation showing the thickness of nanoplatelets in about 28 nm.

[Fig. 2(f)], respectively, reveals complementary image contrast, indicating that the nanoplatelet is actually composed of several diamond crystallites in twin.

C. Composition and chemistry characterization of diamond nanoplatelets

To examine the composition and chemistry of the diamond nanoplatelets, EELS characterization was also used. In Fig. 3(a), the low energy loss EELS spectrum shows a plasmon peak at 34 eV, which is the characteristic peak of diamond. It should be noted that the asymmetrical shape of the peak with a shoulder around the lower energy side is probably contributed from diamond surface plasmon (23 eV), amorphous carbon plasmon (25 eV), and graphite plasmon (27 eV).[18] The thickness of the nanoplatelet is estimated to be about 27 nm by the log-ratio method from the low-loss region of this spectrum. The estimated thickness by EELS is in excellent agreement with side-view SEM observation [Fig. 1(d)]. The near-edge structure of carbon K-edge in EELS [Fig. 3(b)] reveals that the chemical bonding state of the nanoplatelets has predominantly the characteristics of diamond in addition to a small peak at 285 eV corresponding to the π^* orbit of sp^2 carbon as a result of the graphite and amorphous carbon sheath. The EELS analyses show that diamond is the actually major component of the nanoplatelets.

Figure 4(a) shows the BF image of another piece of diamond platelet in the [111] zone axis. Moiré fringes can be clearly observed on the platelet, resulting from interference of two overlapped crystals with close periodicity of lattice spacing. From the enlargement of the black frame in Fig. 4(a), Moiré fringes can be clearly observed [Fig. 4(b)]. The measured angles between the crossed fringes are about 60°, and the spacing of the fringes is about 57.6 Å. According to SAD pattern [inset of Fig. 4(a)], these fringes relate to the diffraction spots of diamond 220 and the graphite $11\bar{2}0$, which have a small difference in interplanar spacing (~0.02 Å). Theoretical calculation of the Moiré fringe spacing between diamond {022} and graphite $\{11\bar{2}0\}$ is about 54.7 Å, which is close to the measured values within experimental error at the operation magnification. The results of diffraction patterns and Moiré fringes show that the crystallographic relationship of the graphite with the diamond is $\langle 111\rangle_{\mathrm{dia}}$ // $\langle 0001\rangle_{\mathrm{graphite}}$ and $\{1\bar{1}0\}_{\mathrm{dia}}$ // $\{11\bar{2}0\}_{\mathrm{graphite}}$. The crystallographic relationship between diamond and graphite, which suggests that the graphite layer epitaxially covers the surfaces of diamond platelets. The same relationship has been observed on the case of diamond epitaxial nucleation on graphite substrate.[19–21] Interestingly, the Moiré fringes disappeared under long period exposure of electron irradiation, implying that the thin graphite layer was damaged by electron beam.

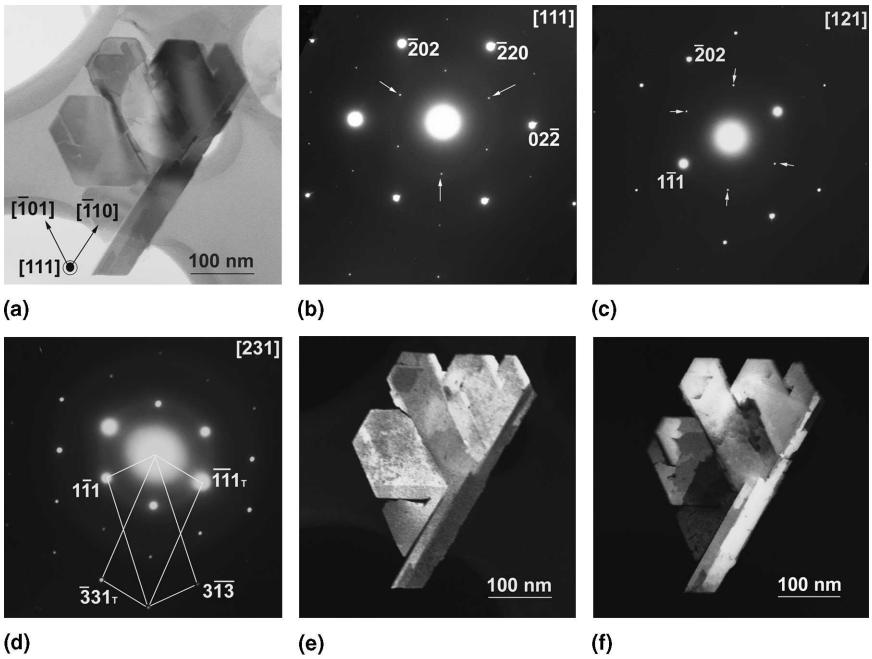

FIG. 2. (a) Typical bright-field TEM image showing a diamond platelet. (b) Corresponding SAD pattern in diamond [111] zone-axis. The white arrowheads indicate 1/3{$\bar{4}$22} forbidden reflections of diamond. (c) SAD pattern in [121] zone-axis after tilting 19.5° from (b). The weak spots marked as white arrowheads are contributed from twins. (d) SAD pattern in [231] zone-axis after tilting 10.9° from (c) showing typical reflections from twinned diamond. (e) Dark-field image taking from the 1$\bar{1}$1 reflection spot in (d). (f) Dark-field image taking from the $\bar{1}\bar{1}1_T$ reflection spot in (d).

Figure 4(c) shows a high-resolution TEM image from an edge region of another diamond nanoplatelet. Graphite {0002} lattice fringes (interplanar spacing of 0.346 nm) and diamond {111} lattice fringes (interplanar spacing of 0.206 nm) are clearly identified. It is observed that about 3–5 layers of graphite {0002} with an amorphous layer cover the side of the diamond platelet. Evans et al. also have observed an ultrathin oriented graphite layer on the diamond {111} face after annealing in a vacuum.[21] Although the explicit reason of graphite formation is not well understood, the formation of graphite is likely a result of high-temperature processing (>1100 °C), which would induce partial graphitization of the diamond on the surface.[22] Alternatively, the formation of a thin graphite layer might result from the residual hydrocarbon radical in the chamber deposited on the diamond platelet after the microwave power was turned off.

D. Characterization of diamond nanoplatelets in the side-view direction

To realize the growth mechanism of platelets in detail, the TEM characterization in the side-view direction of the platelet is vitally important. As the tilting angle in the TEM is limited to 30°, it is impossible to obtain the image of the same platelet in side-on orientation by 90° tilt. Fortunately, some of small platelets were situated on the carbon film in the side-on orientation, which allows

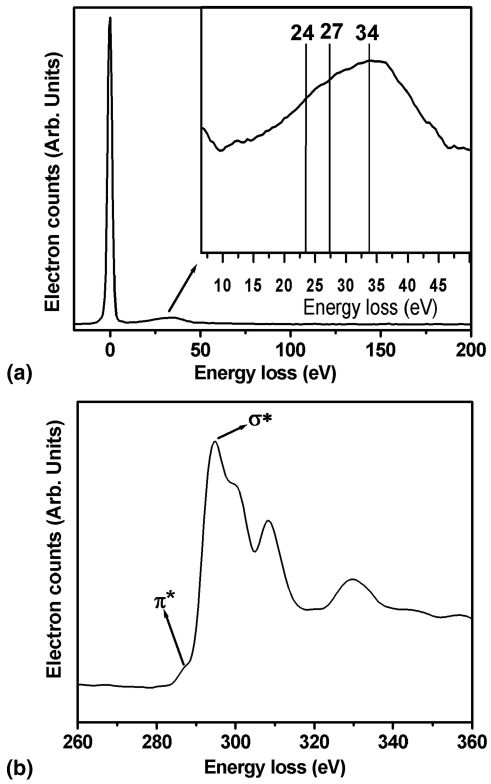

FIG. 3. EELS spectra of diamond nanoplatelet showing (a) low energy-loss region and (b) carbon K edge.

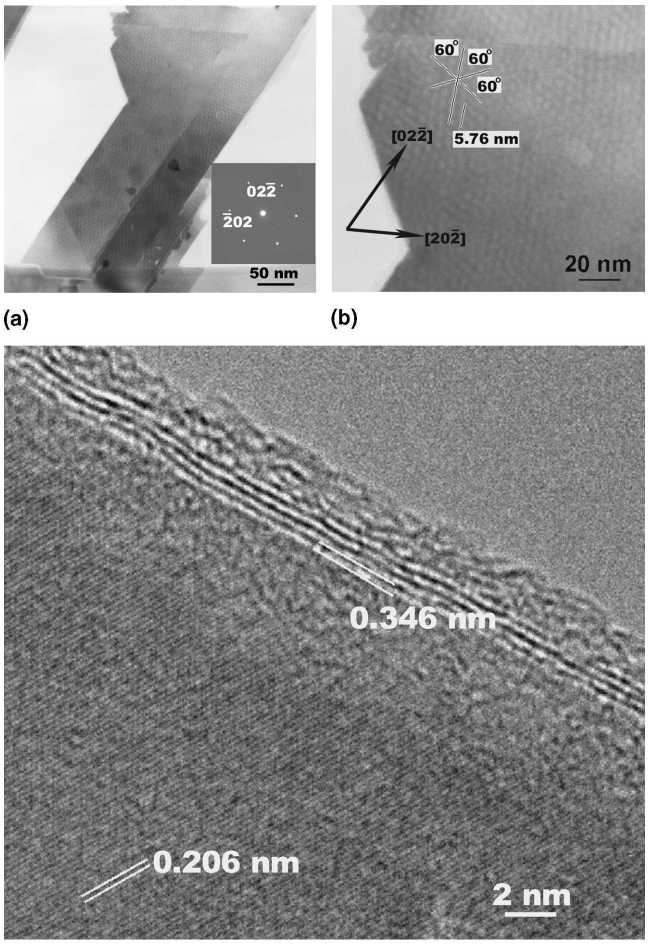

FIG. 4. (a) TEM micrograph showing the diamond platelets; the inset shows the diffraction pattern. (b) Enlargement in (a) showing Moiré fringes. (c) HRTEM micrograph from another platelet revealing a graphite layer covering on diamond platelet surface.

further characterization. In Fig. 5(a), a diamond nanoplatelet was just hung on the periphery of a hole in the supported carbon film in side-on orientation parallel to the TEM optic axis, so that we were able to examine the microstructure in side-view. The thickness of the platelet is approximately 20 nm, which is in good agreement with the SEM observation [Fig. 1(d)]. The SAD pattern [Fig. 5(b)] shows typical twin pattern of diamond in the [01$\bar{1}$] zone-axis and the tabular plane of the diamond platelet parallel to the {111} plane. Because of the shape factor in electron diffraction, the tabular geometry and the twinning in the diamond platelet cause streaks in the pattern along [111] direction. Figure 5(c) shows the DF image taking from the $1\bar{1}\bar{1}_T$ twin spot. It is observed that the diamond consists of multi-parallel twins parallel to the {111} tabular plane of platelet. From the image contrast, there is an ultrathin twin lamella 1 nm thick in the platelet, indicated by small white arrowhead. It is remarkable that the same thin twin lamella in the DF image [see Fig. 5(c)] appears as a dark line in complementary contrast in the bright-field image [see Fig. 5(a)]. Figure 5(d) is the enlarged image of Fig. 5(a) from which the ridge edge structure can be observed. Based on the SAD pattern, the indexing of the facets of the side face of the platelet is schematically drawn in Fig. 5(e). It shows that the side faces consist of {100} and {111} facets. It is believed that a twinning process occurred in a very early stage of diamond deposition and plays critical role for platelet growth. Thus, characterization of the platelet side face's detailed structure is essential to understand the platelet growth mechanism. However, the resolution of conventional TEM image approaches about 1 nm, which makes it difficult to examine the detailed feature of side face structure of the ultrathin twin lamella in atomic resolution. Therefore, high-resolution transmission electron microscopy (HRTEM) was used to characterize the side face structure. A HRTEM micrograph obtained from another diamond nanoplatelet is shown in Fig. 6. Three twin boundaries parallel to the tabulate surfaces can be seen clearly, and they are terminated at the side faces. The thickness of the twinned lamellae is about 2 nm. The inset is a fast Fourier transformation (FFT) pattern of the image, showing the [01$\bar{1}$] zone axis diffraction pattern of twinned diamond. From the pattern and the lattice fringes, a ridge edge side-face structure of $(100)/(100)_T/(1\bar{1}\bar{1})/(100)_T$ faces is evident as illustrated by bold black lines. The angles between these faces are consistent with crystallography as well. Thus, the HRTEM results again confirm the existence of ridge edge structure consisting of (100) and (111) faces. Also, it is noticed that the dislocation density in the diamond nanoplatelets is very low as they are hardly seen in the TEM images we have examined.

IV. DISCUSSION

In common CVD diamond growth, the morphology of isolated diamonds often develops into cubo-octahedral and pyramid shapes by three-dimensional growth as determined by the relative growth rates on {100} and {111} faces.[23] In our case, the habit of diamond platelet via two-dimensional growth exhibits {111} faces. For diamond nanoplatelet, the lateral growth rate is much higher than the growth rate normal to the tabular plane, resulting in a high-aspect-ratio platelet configuration. Although the explicit reason for lateral growth of diamond nanoplatelets is not yet clear, the existence of twins on nanoplatelets provides a possible route for fast growth along the twin plane. The crystal shape of the perfect deposited crystals would be different to that of twinned ones. Various crystal shapes of twinned crystals have been reported by authors. In face-centered-cubic crystal, the multiply-twinned particles displaying 5-fold symmetry usually emerge as decahedra and/or icosahedra under normal

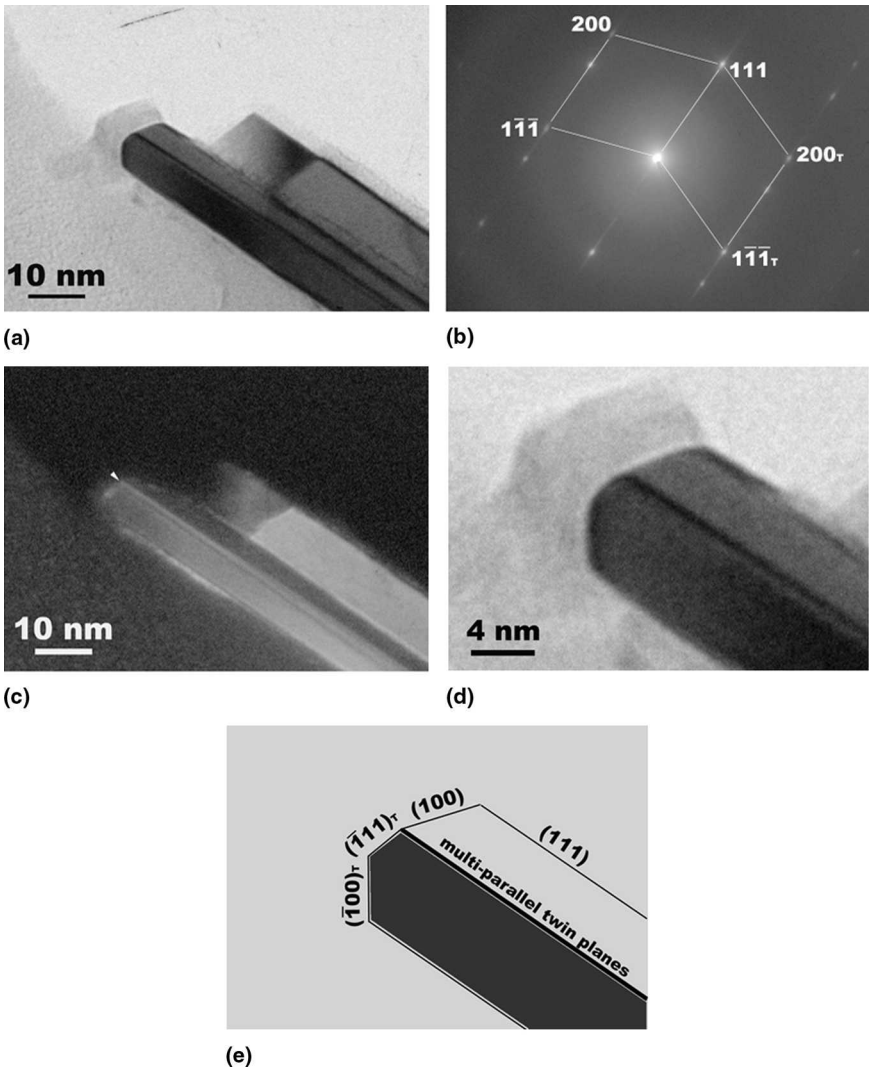

FIG. 5. (a) TEM bright-field image of a diamond platelet hung on the periphery of a hole in the supported carbon film in side-on orientation parallel to TEM optical axis. (b) Corresponding SAD pattern showing typical diamond twin reflections in [01$\bar{1}$] zone-axis. (c) Dark-field image of multi-parallel twins appearing in the diamond nanoplatelet. The white arrowhead indicates an ultrathin twin lamella. (d) Enlarged portion from the BF image of (a) showing appearance of ridge edge on the side face. (e) Schematic illustration showing that the facets of the ridge edge are composed of (111) and (100) faces.

crystal growth conditions. When multi-parallel twinning occurs in a crystal, the platelet can sometimes be observed. Such crystal platelets with parallel twins have already been observed in noble metals,[15] germanium,[24] and silver halides.[25] In the case of diamond, the hexagonal platelet of large micron-sized diamond with a low aspect ratio has been shown by Angus et al.[11] However, the present diamond nanoplatelets with high aspect ratio consist of several tabular crystallites in the shape of trapezoids and parallelograms.

Angus et al. observed the existence of re-entrant edge on the side-face of their platelet and considered that the growth of diamond platelet follows the twinned plane reentrant groove growth model.[11] The twinned plane reentrant groove growth model, which is the widely accepted explanation for the growth of these twinned platelets, was originally proposed by Hamilton and Seidensticker, and they proposed that the side-face of platelet was only bounded by {111} faces.[24] Thus, the side-face structure of the platelet was believed to consist of ridge and trough structure, and the trough structure was believed to exhibit a 141.1° re-entrant groove on the side face, which provides preferential growth sites for the lateral development of platelet. Because the site has higher number of nearest neighbors than flat {111} plane, it is the most likely place for the adatom incorporation and acts as a self-perpetuating step source for lateral growth.[11,26] However, it is not certain if this growth

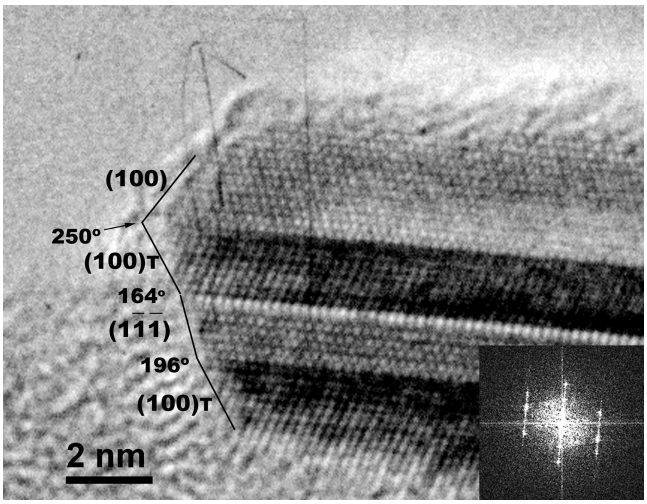

FIG. 6. HRTEM image showing the fine structure of platelet side-face in ridge edge shape, which consists of {111} and {100} faces. The inset shows the corresponding diffraction pattern by the fast Fourier transformation (FFT).

mechanism can be applied to the case of diamond nanoplatelets as no apparent re-entrant grooves on the side face can be seen from the HRTEM image of Fig. 6. In contrast, only a ridge side face structure can be observed. Faceting with ridge side face structure contained {100} and {111} face in CVD diamond crystal has hardly reported before; however, such a ridge side-face structure with {100} and {111} faces has been often found in silver halide crystals, and various ridge side-face structures have been also extensively demonstrated.[25,27–29] Actually, the re-entrant groove only bounded {111} faces is not the sole side-face structure causing the lateral growth of platelet. The different relative growth rate between {111} and {100} would cause the various side-face structure of the twinned platelet, as shown by Bögels et al.[28,29] In silver halide crystal, the slow growth rate of {100} face results in the emergence of {100} face on the side face. Furthermore, Lee et al.[30] used the Monte Carlo method to simulate the development of the side-face structure of a face-centered-cubic twinned crystal platelet under various relative growth rate between {100} and {111} faces. They showed that the twinned plane re-entrant groove only bounded by {111} faces appears in the situation of very high {100} face growth rate, and when the {100} face growth rate is reduced, the ridge-edge side-face structures consisting of {100} and {111} face are major characteristics. Although the growth rate of {100} face is reduced in the above case, the {100} face still has higher growth rate than {111} face, due to the higher number of neighbors for adatoms on the {100} face.

The occurrence of preferential lateral growth in ridge edge side face structure can be rationalized by considering the sub-step model proposed by Ming et al.,[31] which is supported by subsequent experimental evidence.[27–29] The illustration of the sub-step model is shown in Figs. 7(a)–7(f). The model is based on the assumption that {100} faces grow faster than {111}, and it can be recognized that the two-dimensional nucleation easily occurs on the {100}, as illustrated in Fig. 6(b). When the nucleation occurs, a new layer forms and extends to the ridge edge where there is a twin plane. As it occurs, the sub-step then emerges near the ridge edge [Fig. 7(c)], as indicated by black arrows. In case of crystal growth of CVD diamond, the mechanism and chemistry is very distinct from conventional vapor phase crystal growth. For the CVD diamond growth, it has been generally accepted that the surface is predominantly terminated with hydrogen. As the terminated hydrogen can be abstracted by atomic hydrogen in the plasma, the left site is activated with the dangling bonds on the surface. Then the site allows the addition of the reactive hydrocarbon radicals, such as methyl, into C–C bonding in sp^3 bonds, such that the surface is again hydrogen terminated.[32–34] According to simulation in atomic model,[11,34] the formation of a stable surface nucleus on flat {111} face requires three carbon atoms. However, the sub-step atomic model shows only two atoms are required to attach to the site to extend across the twin plane [Fig. 7(e)]. Further growth on {111} sector can proceed, as shown in Fig. 7(f). Therefore, the probability for incorporation of the adatoms at sub-step is very high. After atoms are accommodated at the site, the step flow can easily extend across ridge edge (twin plane) to complete the growth of the {111} layer [Fig. 7(d)]. Thus, the sub-step site in the ridge edge acts as a self-perpetuating step source, resulting in lateral growth. On the {100} face, there are a higher number of neighbors for adatoms which might cause a higher nucleation rate than on {111} face. As a result of sub-step on the side face, {111} growth on the side faces is much easier than it is on the {111} tabular planes. Thus, it can explain that lateral growth of platelet still persists in ridge edge side face structure, even though the side face structure has no re-entrant groove to provide preferential growth site. Therefore, it is recognized that {100} face plays an important role in the lateral growth.[25,27,28]

We have noticed that conventional CVD diamond is synthesized at substrate temperature in the range of 700–900 °C, which is much lower than the present case (>1100 °C). Using the same experimental condition at lower temperature, we found no platelets on the substrate. Thus, it is likely that the high-temperature condition might favor the growth of twinned diamond nanoplatelet. Also, it is well-known that the relative growth rate of {111} and {100} face of diamond significantly depends on growth condition.[23] According to the above arguments, we believe that the ridge edge side-face structure in diamond nanoplatelet, which has rarely observed

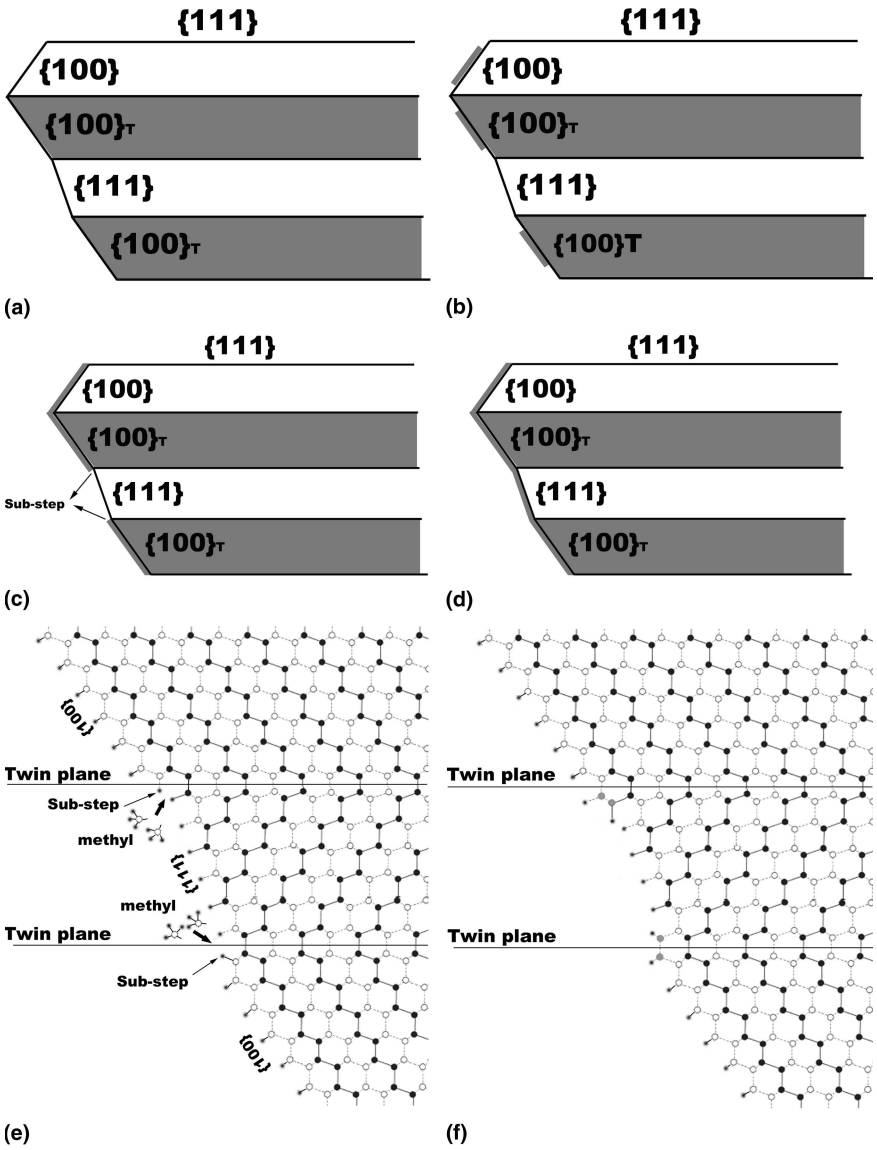

FIG. 7. Schematic illustration showing lateral growth on the ridge edge by the sub-step model: (a) Initial side face structure. (b) Nucleation of a new layer on {100} faces. (c) Emergence of sub-steps when propagation of the new layer reaches the twin edge. (d) Extension of the new layer across the ridge edge (twin plane) due to favorable incorporation of adatoms into sub-step site to complete the growth of the whole layer in lateral direction. (e) Atomic sketch showing the sub-step at the ridge edge projected on {110} plane. The foreign radicals (such as methyl) favorably incorporate into the sub-step sites. Small solid dots represent hydrogen atoms; open circles represent carbon atoms; and solid circles represent carbon atoms in different layers. (f) Incorporation of two carbon atoms into the sub-step site. The new layer can then extend across ridge edge (twin plane) and further sustain the growth on {111} sector.

before is closely related with the significantly different growth condition (relative growth rate of {100} and {111} faces, high processing temperature, and chemical reaction, etc.).

The droplets of Ni in several tens of nanometers were also seen by TEM and SEM (not shown), while no Ni in diamond platelets was detected by x-ray energy dispersive spectroscopy and EELS. The influence of Ni on formation of diamond nanoplatelets is still unknown at the moment and will be clarified in future work.

V. CONCLUSIONS

Single-crystalline diamond nanoplatelets 30 nm thickness were synthesized on Ni-coated polycrystalline diamond substrate by the MPCVD process at 1100 °C. Characterization of SEM and TEM indicates that the diamond nanoplatelets appear in a specific shape consisting of several trapezoid and parallelogram tabular crystallites. Electron diffraction verifies that the top and bottom tabular planes of the platelet are {111} face and the edges of nanoplatelets are along the ⟨110⟩ directions. The

multi-parallel twins in diamond platelets were revealed by plan-view and side-view TEM observations. The presence of twins with a ridge side face structure is essential for the lateral growth of diamond nanoplatelets. From EELS characterization, it is evident that diamond is the major component of the nanoplatelets. An oriented thin graphite layer is also observed on some nanoplatelets.

ACKNOWLEDGMENT

We thank the support from National Science Council, Taiwan, Republic of China, under Contract No. NSC 91-2216-E-009-014.

REFERENCES

1. J. Isberg, J. Hammersberg, E. Johansson, T. Wikström, D.J. Twitchen, A.J. Whitehead, S.E. Coe, and G.A. Scarsbrook: High carrier mobility in single-crystal plasma-deposited diamond. *Science* **297,** 1670 (2002).
2. W.S. Yang, O. Auciello, J.E. Butler, W. Cai, J.A. Carlisle, J. Gerbi, D.M. Gruen, T. Knickerbocker, T.L. Lasseter, J.N. Russell, L.M. Smith, and R.J. Hamers: DNA-modified nanocrystalline diamond thin-films as stable, biologically active substrates. *Nat. Mater.* **1,** 253 (2002).
3. O. Shenderova, D. Brenner, and R.S. Ruoff: Would diamond nanorods be stronger than fullerene nanotubes. *Nano Lett.* **3,** 805 (2003).
4. O.A. Shenderova, V.V. Zhirnov, and D.W. Brenner: Carbon nanostructures. *Crit. Rev. Solid State Mater. Sci.* **27,** 227 (2002).
5. K. Kobashi, T. Tachibana, Y. Yokota, N. Kawakami, K. Hayashi, and K. Inoue: Formation of fibrous structures on diamond by hydrogen plasma treatment under DC bias. *Diamond Relat. Mater.* **10,** 2039 (2001).
6. E.S. Baik, Y.J. Baik, S.W. Lee, and D. Jeon: Fabrication of diamond nano-whiskers. *Thin Solid Films* **377-378,** 295 (2000).
7. H. Masuda, T. Yanagishita, K. Yasui, K. Nishio, I. Yagi, T.N. Rao, and A. Fujishima: Synthesis of well-aligned diamond nanocylinders. *Adv. Mater.* **13,** 247 (2001).
8. J.O. Orwa, S. Prawer, D.N. Jamieson, J.L. Peng, J.C. McCallum, K.W. Nugent, Y.J. Li, L.A. Bursill, and S.P. Withrow: Diamond nanocrystals formed by direct implantation of fused silica with carbon. *J. Appl. Phys.* **90,** 3007 (2001).
9. D.M. Gruen: Nanocrystalline diamond films. *Annu. Rev. Mater. Sci.* **29,** 211 (1999).
10. J. Philip, P. Hess, T. Feygelson, J.E. Butler, S. Chattopadhyay, K.H. Chen, and L.C. Chen: Elastic, mechanical, and thermal properties of nanocrystalline diamond films. *J. Appl. Phys.* **93,** 2164 (2003).
11. J.C. Angus, M. Sunkara, S.R. Sahaida, and J.T. Glass: Twinning and faceting in early stage of diamond growth by chemical vapor deposition. *J. Mater. Res.* **7,** 3001 (1992).
12. S. Iijima: Observation of atomic steps of (111) surface of a silicon crystal using bright fields electron microscopy. *Ultramicroscopy* **6,** 41 (1981).
13. X. Chen and J.M. Gibson: Measurement of roughness at buried Si/SiO_2 interfaces by transmission electron diffraction. *Phys. Rev. B* **54,** 2846 (1996).
14. D. Cherns: Direct resolution of surface atomic steps by transmission electron microscopy. *Philos. Mag.* **30,** 549 (1974).
15. A.I. Kirkland, D.A. Jefferson, D.G. Duff, P.P. Edwards, I. Gameson, B.F.G. Johnson, and D.J. Smith: Structural studies of trigonal lamellar particles of gold and silver. *Proc. R. Soc. London, Ser. A* **440,** 589 (1993).
16. Z.L. Wang, J. Bentley, R.E. Clausing, L. Heatherly, and L.L. Horton: Direct correlation of microtwin distribution with growth face morphology of CVD diamond films by a novel TEM technique. *J. Mater. Res.* **9,** 1552 (1994).
17. P.B. Hirsch, A. Howie, R.B. Nicholoson, D.W. Pashley, and M.J. Whelan: *Electron Microscopy of Thin Crystals* (Butterworths, London, U.K., 1965), pp. 143–144.
18. A. Duarte-Moller, F. Espinosa-Magaña, R. Martinez-Sanchez, M. Avalos-Borja, G.A. Hirata, and L. Cota-Araiza: Study of different forms of carbon by analytical electron microscopy. *J. Electron Spectrosc.* **104,** 61 (1999).
19. W.R.L. Lambrecht, C.H. Lee, B. Segall, J.C. Angus, Z. Li, and M. Sunkara: Diamond nucleation by hydrogenation of the edges of graphitic precursors. *Nature* **364,** 607 (1993).
20. Z. Li, L. Wang, T. Suzuki, A. Argoitia, P. Pirouz, and J.C. Angus: Orientation relationship between chemical-vapor-deposition diamond and graphite substrates. *J. Appl. Phys.* **73,** 711 (1993).
21. T. Evans: Changes produced by high temperature treatment of diamond, in *The Properties of Diamond,* edited by J.E. Field (Academic Press, London, U.K., 1979), pp. 403–424.
22. G. Jungnickel, D. Porezag, T. Frauenheim, M.I. Heggie, W.R.L. Lambrecht, B. Segall, and J.C. Angus: Graphitization effects on diamond surfaces and the diamond graphite interface. *Phys. Status Solidi A* **154,** 109 (1996).
23. C. Wild, R. Kohl, N. Herres, W. Müller-Sebert, and P. Koidl: Oriented CVD diamond films-twin formation, structure and morphology. *Diamond Relat. Mater.* **3,** 373 (1994).
24. D.R. Hamilton and R.G. Seidensticker: Propagation mechanism of germanium denfrites. *J. Appl. Phys.* **31,** 1165 (1960).
25. R. Jagannathan, R.V. Mehta, J.A. Timmons, and D.L. Black: Anisotropic growth of twinned cubic crystals. *Phys. Rev. B* **48,** 13261 (1993).
26. J.W. Steeds, A.E. Mora, J.E. Butler, and K.M. Bussmann: Transmission electron microscopy investigation of boron-doped polycrystalline chemically vapor-deposited diamond. *Philos. Mag. A* **82,** 1741 (2002).
27. G. Bögels, T.M. Pot, H. Meekes, P. Bennema, and D. Bollen: Side-face structure and growth mechanism of tabular silver bromide crystals. *Acta Crystallogr. A* **53,** 84 (1997).
28. G. Bögels, H. Meekes, P. Bennema, and D. Bollen: The role of {100} side faces for lateral growth of tabular silver bromide crystals. *J. Cryst. Growth* **191,** 446 (1998).
29. G. Bögels, H. Meekes, P. Bennema, and D. Bollen: Twin formation and morphology of vapour growth silver halide crystals. *Philos. Mag. A* **79,** 639 (1998).
30. J.W. Lee, N.M. Hwang, and D.Y. Kim: Growth morphology of perfect and twinned faced-centered-cubic crystals by Monte Carlo simulation. *J. Cryst. Growth* **250,** 538 (2003).
31. N.B. Ming and I. Sunagawa: Twin lamellae as possible self-perpetuating step sources. *J. Cryst. Growth* **87,** 13 (1988).
32. K. Larsson, S. Lunell, and J.O. Carlsson: Adsorption of hydrocarbons on a diamond (111) surface: An initio quantum-mechanical study. *Phys. Rev. B* **48,** 2666 (1993).
33. H. Tamura, H. Zhou, Y. Hirano, S. Takami, M. Kubo, R.V. Belosludov, A. Miyamoto, A. Imamura, N.M. Gamo, and T. Ando: First-principle study on reactions of diamond (100) surfaces with hydrogen and methyl radicals. *Phys. Rev. B* **62,** 16995 (2000).
34. M. Grujicic and S.G. Lai: Atomistic simulation of chemical vapor deposition of (111)-oriented diamond film using a kinetic Monte Carlo method. *J. Mater. Sci.* **34,** 7 (1999).